Title

Publisher Correction: Role of the BUB3 protein in phragmoplast microtubule reorganization during cytokinesis

Journal

Nature Plants, 4(9)

ISSN

2055-026X

Authors

Zhang, Hongchang
Deng, Xingguang
Sun, Baojuan
et al.

Publication Date

2018-09-01

DOI

10.1038/s41477-018-0215-9

Peer reviewed

nature plants

ARTICLES

https://doi.org/10.1038/s41477-018-0192-z

Corrected: Publisher Correction

Role of the BUB3 protein in phragmoplast microtubule reorganization during cytokinesis

Hongchang Zhang[1,2,6], Xingguang Deng[2,3,6], Baojuan Sun[2,4], Sonny Lee Van[2], Zhensheng Kang[5], Honghui Lin[3], Yuh-Ru Julie Lee[2*] and Bo Liu[2*]

The evolutionarily conserved WD40 protein budding uninhibited by benzimidazole 3 (BUB3) is known for its function in spindle assembly checkpoint control. In the model plant *Arabidopsis thaliana*, nearly identical BUB3;1 and BUB3;2 proteins decorated the phragmoplast midline through interaction with the microtubule-associated protein MAP65-3 during cytokinesis. BUB3;1 and BUB3;2 interacted with the carboxy-terminal segment of MAP65-3 (but not MAP65-1), which harbours its microtubule-binding domain for its post-mitotic localization. Reciprocally, BUB3;1 and BUB3;2 also regulated MAP65-3 localization in the phragmoplast by enhancing its microtubule association. In the *bub3;1 bub3;2* double mutant, MAP65-3 localization was often dissipated away from the phragmoplast midline and abolished upon treatment of low doses of the cytokinesis inhibitory drug caffeine that were tolerated by the control plant. The phragmoplast microtubule array exhibited uncoordinated expansion pattern in the double mutant cells as the phragmoplast edge reached the parental plasma membrane at different times in different areas. Upon caffeine treatment, phragmoplast expansion was halted as if the microtubule array was frozen. As a result, cytokinesis was abolished due to failed cell plate assembly. Our findings have uncovered a novel function of the plant BUB3 in MAP65-3-dependent microtubule reorganization during cytokinesis.

Budding uninhibited by benzimidazole 3 (BUB3) is a WD40 repeat protein that is highly conserved among eukaryotic organisms[1]. In fungi and animals, BUB3 is an essential component of the spindle assembly checkpoint (SAC), which ensures that all sister chromatids are attached to kinetochore fibres originating from opposite poles of the bipolar spindle before anaphase onset. Before satisfying such a biorientation, the SAC is activated and BUB3 interacts with a conserved Gle-binding site (GLEBS) domain in the BUB1 and the BUB1-related protein 1 (BUBR1; also known as mitotic arrest defect 3 (MAD3)) proteins to ultimately inhibit the anaphase-promoting complex or cyclosome[2]. When the SAC mechanism is dismantled, mitosis proceeds without having all of the chromosomes properly aligned. In fungi, mutants that are defective in the SAC become hypersensitive to microtubule-depolymerizing drugs, with low doses causing lethality[1,3]. In mammals, the loss of the *BUB3* gene leads to embryonic lethality[4].

The model flowering plant *Arabidopsis thaliana* has homologous genes encoding BUB1, BUBR1 and BUB3-like proteins[5,6]. Surprisingly, all the plant BUB1/MAD3 family proteins 1/2/3 (also known as BMF1/2/3) lack the canonical BUB3-interacting GLEBS domain, and upon SAC activation, decorate spindle microtubules instead of kinetochores[6]. Three BUB3 proteins are encoded by the *A. thaliana* genome: nearly identical BUB3;1 and BUB3;2 display high sequence identity to BUB3 proteins from other kingdoms, whereas BUB3;3 is more divergent[6]. A mutant carrying a transfer DNA (T-DNA) insertion in the *BUB3;1* gene was reported to cause female gametophytic lethality[6]. However, the linkage between the genotype and the phenotype has not been demonstrated by means of genetic suppression or complementation tests. Furthermore, BUB3;1 and BUB3;2 probably play redundant roles according to their nearly identical amino acid sequences and similar expression patterns that are evident in tissues enriched with actively dividing cells (http://jsp.weigelworld.org/expviz/expviz.jsp).

An earlier systematic query for proteins interacting with important factors of the cell cycle has uncovered a surprising interaction between BUB3;2 and the microtubule-associated protein MAP65-3 by the yeast two-hybrid assay[7]. MAP65-3 is a cytokinesis-specific MAP65 isoform in *A. thaliana* and functions in crosslinking or bundling antiparallel microtubules in the spindle midzone during late anaphase and in the phragmoplast midline during cytokinesis[8–10]. Furthermore, upon overexpression in tobacco cells or when expressed in *A. thaliana*, green fluorescent protein (GFP) fusion with the *Arabidopsis* BUB3;1 decorates the phragmoplast midline in cytokinetic cells[5,6]. This further supports the in vivo BUB3;1–MAP65-3 association, although the authenticity of the association would need to be verified in the plant from which the proteins are identified. Nevertheless, these lines of evidence, together with the fact that *Arabidopsis* BMF proteins lack the GLEBS domain, suggest that plant BUB3 proteins may not exercise similar functions in mitosis as their fungal and animal counterparts. Instead, they were proposed to play a role in the phragmoplast during cytokinesis.

To test this hypothesis, we isolated mutants carrying T-DNA insertions at the *BUB3;1* and *BUB3;2* loci in *A. thaliana* and found that even double homozygous mutant plants grew indistinguishably from the wild-type control. The BUB3;1/BUB3;2-GFP fusion proteins, when expressed under their endogenous promoter in their corresponding mutation backgrounds, demonstrated dynamic redistribution from interphase nuclei to microtubules in the spindle midzone during late stages of anaphase and the phragmoplast midline during cytokinesis. The *bub3;1 bub3;2* double mutant exhibited

[1]State Key Laboratory of Crop Stress Biology for Arid Areas and College of Life Sciences, Northwest A&F University, Yangling, Shaanxi, China. [2]Department of Plant Biology, College of Biological Sciences, University of California, Davis, CA, USA. [3]College of Life Sciences, Sichuan University, Chengdu, Sichuan, China. [4]Vegetable Research Institute, Guangdong Academy of Agricultural Sciences, Guangzhou, Guangdong, China. [5]State Key Laboratory of Crop Stress Biology for Arid Areas and College of Plant Protection, Northwest A&F University, Yangling, Shaanxi, China. [6]These authors contributed equally: Hongchang Zhang, Xingguang Deng. *e-mail: yjlee@ucdavis.edu; bliu@ucdavis.edu

a phenotype of uncoordinated phragmoplast expansion and cytokinesis became hypersensitive to the cytokinesis-disturbing drug caffeine. Thus, these findings provide compelling evidence that the plant BUB3 protein has acquired distinct roles in phragmoplast-based cytokinesis.

Results

To determine the localization of physiologically relevant quantities of BUB3;1 and BUB3;2, their fusions with GFP were expressed under the control of their own promoters. BUB3;1-GFP localized to the nuclei in interphase cells (arrows, Fig. 1A,a) and became diffuse following nuclear envelope breakdown (asterisk, Fig. 1A,a). When mitosis progressed, BUB3;1-GFP became concentrated in the middle region of the cell, as if decorating the bundles of microtubules in the spindle midzone (arrowheads at 340 s, Fig. 1A,b and Supplementary Video 1). Such broadly localized signal was later gradually narrowing down and became concentrated in the midplane of the dividing cell, towards the centre (arrowheads, Fig. 1A,b and Supplementary Video 1). The signal later expanded towards the periphery, concomitantly with its appearance and concentration in the reformed daughter nuclei (arrows, Fig. 1A,b and Supplementary Video 1). Similarly, BUB3;2-GFP, when expressed under the native *BUB3;2* promoter, was detected in the interphase nucleus and the midzone of cells undergoing cytokinesis (data not shown), similarly to what was reported earlier[5]. This result suggests that BUB3;1 and BUB3;2 act similarly during cell division in *A. thaliana* as one would predict from their nearly identical amino acid sequences. Because BUB3;1 and BUB3;2 are nearly identical in their primary amino acid sequences and exhibit identical localization in the phragmoplast midzone, our following analyses were focused on BUB3;1.

We then performed dual localization of BUB3;1 and microtubules by immunofluorescence. BUB3;1-GFP was found to be concentrated in the midline of the phragmoplast microtubule array following the establishment of clear bipolarity (Fig. 1B,a). It appeared in both the phragmoplast midline and the daughter nuclei (Fig. 1B,b). Thus, BUB3;1 localizes at or near the plus ends of phragmoplast microtubules during cytokinesis, where MAP65-3 is also detected[10].

We took a step further to determine the spatial relationship between BUB3;1 and MAP65-3 in dividing cells. In cells that are towards the end of anaphase, BUB3;1-GFP just became discernible in the spindle midzone when MAP65-3 was already abundantly present in a concentrated manner and probably being associated with microtubule bundles (Fig. 1C,a). This result indicates that MAP65-3 decorates microtubules in the spindle midzone before BUB3;1 or BUB3;2. When MAP65-3 became restricted at the midline in the phragmoplast, BUB3;1 exhibited a similar localization pattern (Fig. 1C,b). These in vivo data support the notion that MAP65-3 and BUB3;1 or BUB3;2 interact in developing phragmoplasts.

We went on to examine the interaction between BUB3;1 and MAP65-3 as suggested by the yeast two-hybrid assay[7]. First, we tested whether BUB3;1 interacted with MAP65-3 or with other MAP65 isoforms, as well using a modified bimolecular fluorescence complementation (BiFC) assay as described previously[11]. It was found that BUB3;1 established BiFC with MAP65-3 and generated a yellow fluorescence signal along cortical microtubules that was emitted by the reconstituted Citrine fluorophore, similar to the positive BiFC established by MAP65-3 homodimerization (Fig. 2A,B). No Citrine signal was detected when BUB3;1 bound to a carboxy-terminal Citrine fragment (BUB3;1-cCitrine) and MAP65-1 bound to an amino-terminal Citrine fragment (MAP65-1-nCitrine) were co-expressed in tobacco cells (Fig. 2B). Thus, the BUB3–MAP65 interaction is apparently isoform specific.

We then dissected which domain(s) in MAP65-3 were responsible for the interaction. Because the MAP65 family proteins can

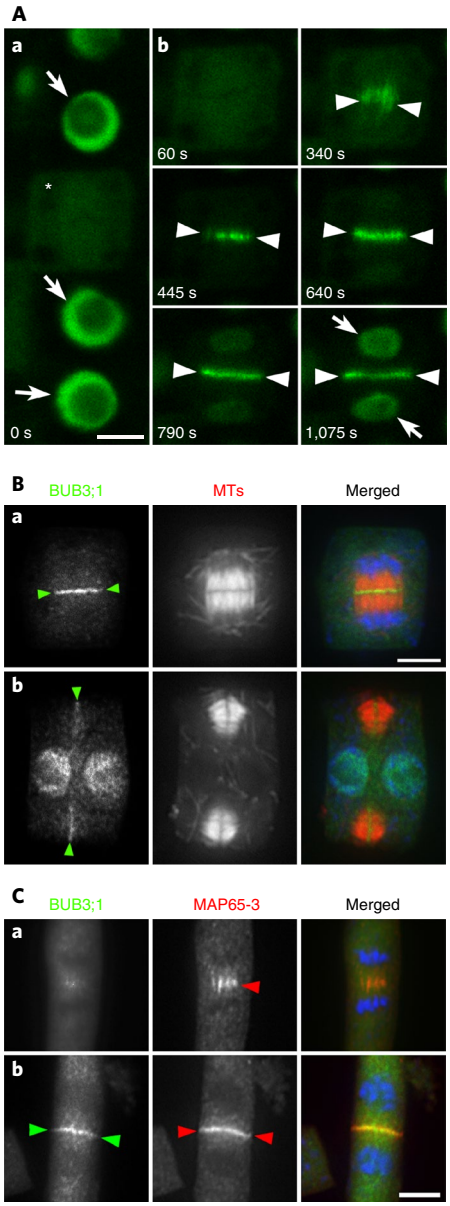

Fig. 1 | BUB3;1 colocalizes with MAP65-3 in the phragmoplast midline. **A**, BUB3;1-GFP in living cells. The BUB3;1-GFP signal is detected in interphase nuclei (arrows) and in the cytosol after nuclear envelope breakdown (asterisk) (**Aa**). Snapshots of BUB3;1-GFP at late stages of mitosis and cytokinesis in the cell highlighted by the asterisk in **Aa** are shown (**Ab**). In **Ab**, the arrowheads point at the concentration of BUB3;1-GFP in the spindle midzone (340 s) and the phragmoplast midline (after 445 s). Towards later stages of cytokinesis, BUB3;1-GFP returns to the reforming daughter nuclei (arrows, 1,075 s). **B**, Triple localization of BUB3;1 (green), microtubules (MTs, red) and DNA (blue) in cells undergoing cytokinesis with the indicated colours in the merged images. BUB3;1 is highly concentrated in the phragmoplast midline (arrowheads) when the bipolar microtubule array is discerned (**Ba**). At later stages, BUB3;1 remains in the midline of the expanding microtubule array (arrowheads) and enters the reforming nuclei (**Bb**). **C**, Triple localization of BUB3;1 (green), MAP65-3 (red) and DNA (blue) in cells undergoing cytokinesis with the indicated colours in the merged images. BUB3;1 is barely detected in the anaphase spindle midzone when MAP65-3 is abundantly detected as if on the microtubule bundles (red arrowheads; **Ca**). At later stages of cytokinesis, the two signals overlap well (green and red arrowheads; **Cb**). Experiments in **A** were repeated independently five times and three times in **B** and **C** with similar results. Scale bars, 5 μm.

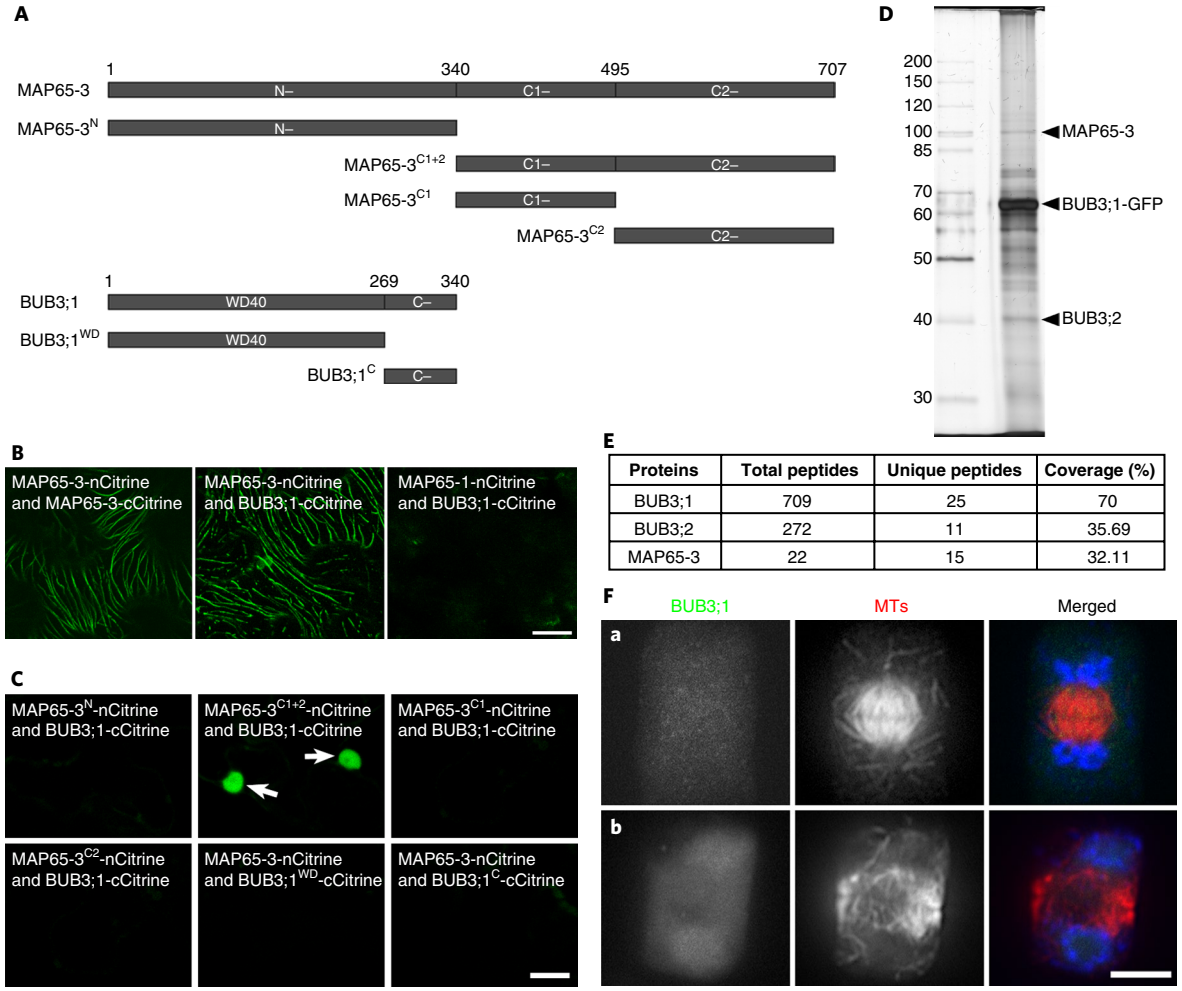

Proteins	Total peptides	Unique peptides	Coverage (%)
BUB3;1	709	25	70
BUB3;2	272	11	35.69
MAP65-3	22	15	32.11

Fig. 2 | BUB3;1 interacts with MAP65-3 for its phragmoplast localization. A, An illustration of the full-length MAP65-3 and BUB3;1 polypeptides and the derived fragments that are used in the BiFC tests shown in panel **C**. BUB3;1^{WD}, BUB3;1 truncation with the WD40 repeats only. **B**, BUB3;1 interacts with MAP65-3 in BiFC. Fluorescent signals decorating the cortical microtubules are reconstituted by nCitrine and cCitrine fragments when they are both fused with MAP65-3 that serve as the positive control because of self-dimerization. MAP65-3-nCitrine, but not MAP65-1-nCitrine, and BUB3;1-cCitrine restore yellow fluorescence due to BiFC. **C**, Only full-length BUB3;1 interacts with MAP65-3^{C1+2}. The reconstituted fluorescent signal is detected exclusively in the nuclei (arrows) due to the nuclear localization of BUB3;1. **D**, Immunopurification of the bait protein BUB3;1-GFP. MAP65-3 and BUB3;2 are co-purified with the bait (arrowheads) in the right lane. The left lane includes the molecular weight markers in kDa (shown to the left). **E**, BUB3;1, BUB3;2 and MAP65-3 are detected by mass spectrometry-assisted peptide identification. The table illustrates the total peptides, unique peptides and coverages of the proteins by the identified peptides. **F**, MAP65-3-dependent BUB3;1 localization. In the *map65-3*-mutant cells undergoing cytokinesis, BUB3;1 is no longer detected at early (**Fa**) or late (**Fb**) stages of phragmoplast development when bipolar microtubule arrays can be discerned. MTs, red; DNA, blue in merged images. Experiments in **B**, **C** and **F** were repeated independently three times and two times in **D** with similar results. Scale bars, 20 μm (**B** and **C**) and 5 μm (**F**).

be roughly divided into the amino-terminal dimerization segment (MAP65-3^{N}) and the carboxy-terminal microtubule-binding part (MAP65-3^{C})[12], we found that no interaction took place between the dimerization domain MAP65-3^{N} and BUB3;1 (Fig. 2C). A positive Citrine signal was detected in the nuclei when BUB3;1-cCitrine was co-expressed with MAP65-3^{C1+2}-nCitrine, indicating the interaction between the two fusion proteins (Fig. 2C). The nuclear localization further supported the interaction because the C1 + 2 fragment of MAP65-3 (MAP65-3^{C1+2}), including amino acids 341–707, would normally decorate cortical microtubules[11]. As BUB3;1 localizes to interphase nuclei[6], the interaction recruited MAP65-3^{C1+2} to the nuclei. Further division of the C-terminal segment into the C1 and C2 domains, as analysed by our previous study[11], indicated that the interaction required the entire C-terminal segment (Fig. 2C).

Because the BUB3 family proteins contain a short C-terminal fragment following the signature WD40 repeats, we asked whether this extension was required for the interaction. We found that the deletion of the C-terminal 71 amino acids completely abolished the interaction and that this fragment did not interact with MAP65-3 (Fig. 2C). Thus, we concluded that the interaction requires both the WD40 repeats and the C-terminal fragment of BUB3;1.

To take one step further, we tested the association of MAP65-3 with BUB3;1 in vivo by immunoaffinity purification. When the bait BUB3;1-GFP was captured by an anti-GFP antibody, specific bands were detected at predicted positions for MAP65-3 and BUB3 in addition to this bait protein (Fig. 2D). We determined purified polypeptides by mass spectrometry-assisted peptide identification using augmin purification[13] as a negative control. Although the bait BUB3;1 was detected with a 70% peptide coverage, MAP65-3 and BUB3;2 were detected at 32.11% and 35.69% coverages, respectively (Fig. 2E, Supplementary Fig. 1 and Supplementary Table 2). The recovery of BUB3;2 together with BUB3;1 suggested that the MAP65-3 dimer probably recruited both isoforms. All three proteins were never recovered in numerous purifications of the

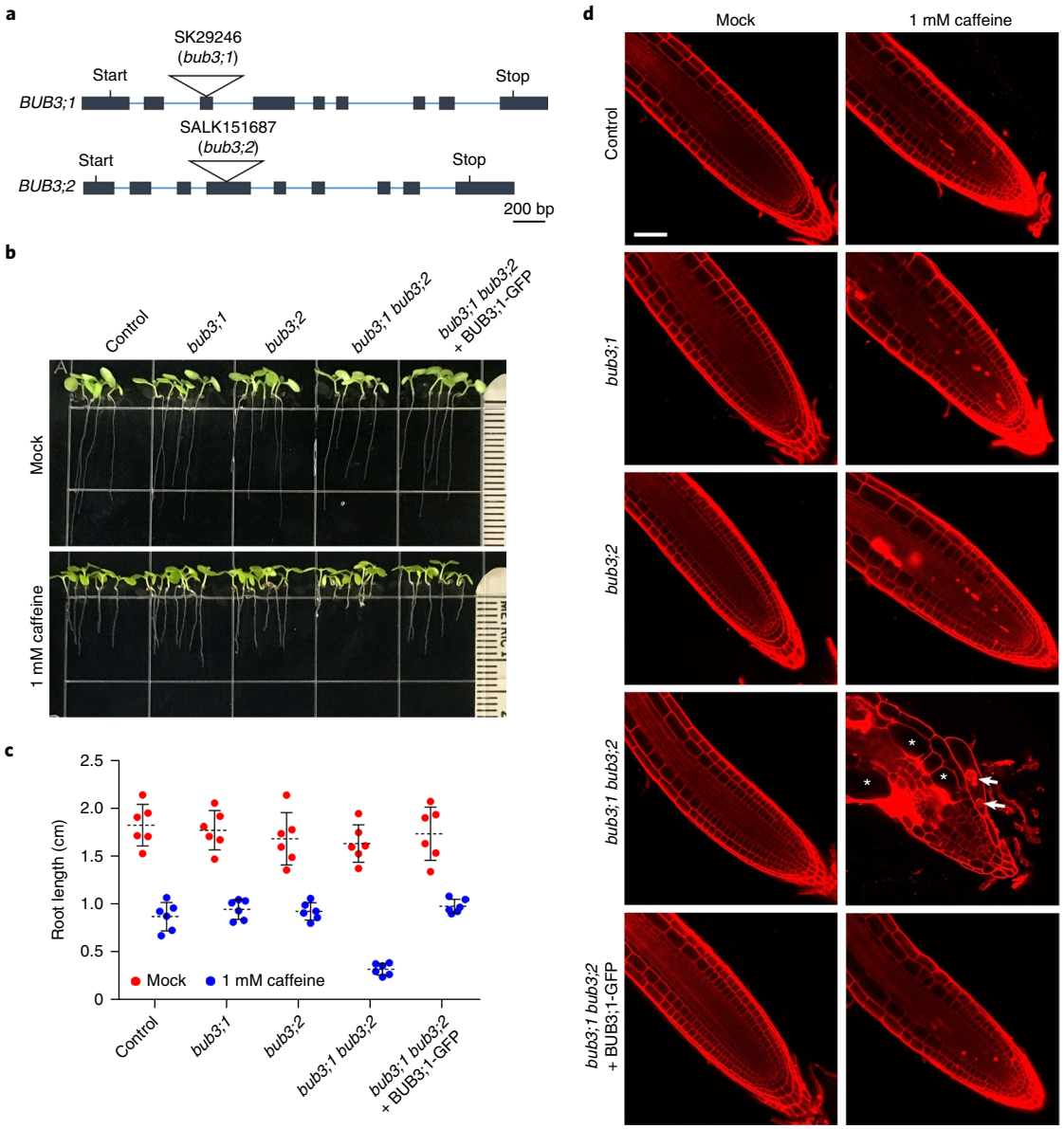

Fig. 3 | *BUB3;1* and *BUB3;2* are functionally redundant. **a**, Schematic representation of T-DNA insertional mutations at the *BUB3;1* and *BUB3;2* loci. The exons (solid boxes), introns (blue lines) and the start and stop codon positions are indicated. **b**, Seedling growth patterns of the wild-type control, *bub3;1* single mutant, *bub3;2* single mutant, *bub3;1bub3;2* double mutant and *bub3;1bub3;2* double mutant expressing BUB3;1-GFP with and without 1 mM caffeine treatment. The smallest unit in the rulers is 1 mm. Only the double mutant has greatly shortened roots with caffeine compared to the control and other mutants, and the phenotype is completely suppressed by BUB3;1-GFP expression. **c**, Quantification of root lengths in the seedlings in panel **b** with and without 1 mM caffeine treatment ($n = 6$ for each sample). The root lengths of control, *bub3;1* single mutant, *bub3;2* single mutant, *bub3;1bub3;2* double mutant and *bub3;1bub3;2* double mutant expressing BUB3;1-GFP are 1.82 ± 0.22, 1.77 ± 0.20, 1.68 ± 0.27, 1.63 ± 0.20 and 1.73 ± 0.28 cm (mean ± s.d.), respectively, without caffeine treatment, and are 0.88 ± 0.15, 0.94 ± 0.10, 0.92 ± 0.10, 0.32 ± 0.06 and 0.98 ± 0.07 cm, respectively, after 1 mM caffeine treatment. **d**, Cell profiles shown by propidium iodide staining near the root-tip regions of the control *bub3;1* single mutant, *bub3;2* single mutant, *bub3;1bub3;2* double mutant and *bub3;1bub3;2* double mutant expressing BUB3;1-GFP with and without 1 mM caffeine treatment. Only the double mutant produced giant cells (asterisks) and had multiple nuclei labelled (arrows) in a single cell. Experiments in **d** were repeated independently three times with similar results. Scale bar, 50 μm (**d**).

augmin complex using GFP-tagged AUG subunits[13]. Thus, we conclude that BUB3;1/BUB3;2 and MAP65-3 specifically associate with each other in vivo.

Because our results suggested that MAP65-3 appeared at the spindle midzone at late anaphase before BUB3;1, we tested whether BUB3;1 localization depended on MAP65-3, as the latter harbours a microtubule-binding site. When BUB3;1-GFP was expressed in the *map65-3-1* mutation background, it no longer concentrated in the midline of the developing phragmoplasts (Fig. 2F).

To determine whether the phragmoplast localization of BUB3;1 and BUB3;2 had functional implications, we isolated mutants harbouring T-DNA insertions in exons toward the 5′ side of both genes (Fig. 3a). Homozygous *bub3;1* and *bub3;2* single mutants did not exhibit noticeable growth defects and neither did the *bub3;1 bub3;2* double mutant (Fig. 3b). We then applied caffeine, a commonly used inhibitor of phragmoplast-based cytokinesis in plants[14], to test whether the isolated mutants exhibited sensitivities that were different from those in the control plant. Although single

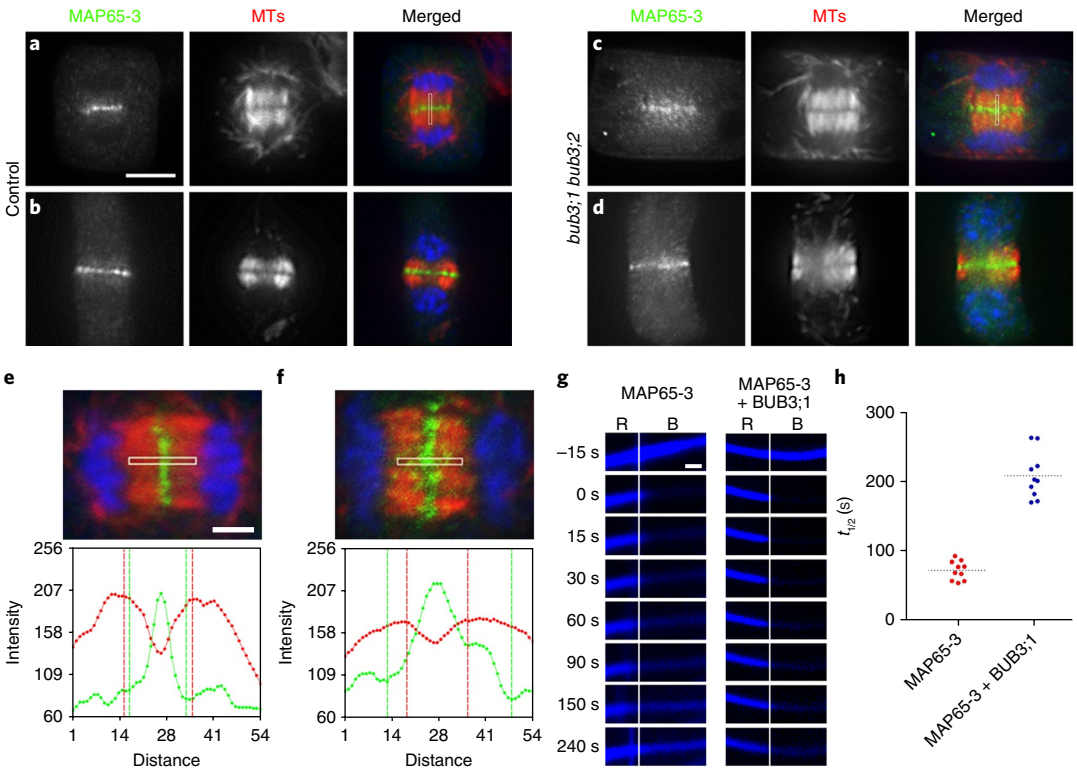

Fig. 4 | BUB3 proteins regulate MAP65-3 localization. **a**,**b**, In the control cells, MAP65-3 exclusively decorates the phragmoplast midline when bipolar microtubule (MT) arrays are detected at early (**a**) and late (**b**) stages. **c**,**d**, In the *bub3;1 bub3;2* double mutant cells, punctate signals of MAP65-3 can be detected along phragmoplast microtubules, away from the midline in both early (**c**) and late (**d**) phragmoplasts. **e**,**f**, Assessment of MAP65-3 distribution patterns in the control (**e**) and *bub3;1 bub3;2* double mutant (**f**) by fluorescence intensity scans of the regions indicated by white rectangles in merged images (**a**–**f**). Enlarged images (top panels) of the merged micrographs in panels **a** and **c**, respectively, have the highlighted regions scanned and the results are shown on the bottom panels. The edges of the phragmoplast midline are illustrated by vertical red lines, and the lowest MAP65-3 points are highlighted by vertical green lines. The MAP65-3 signal has a much wider peak across the phragmoplast. In the merged images (**a**–**f**), MAP65-3 is pseudo-coloured in green, microtubules in red and DNA in blue. **g**, MAP65-3 turnovers on microtubule bundles in the absence or presence of BUB3;1. FRAP of CFP-MAP65-3 when it is expressed alone (left) or co-expressed with BUB3;1 (right) is shown. Both signals of the neighbouring reference (R) and pre-bleaching-bleaching-recovery (B) were taken at the time points shown on the left. **h**, FRAP of CFP-MAP65-3 alone or with RFP-BUB3;1 had a $t_{1/2}$ averaged at 72.34 s and 208.14 s, respectively (indicated by the dotted line; $n = 10$ biologically independent samples for each measurement). The difference is obvious because no values overlap in the two tests. Experiments in **a**–**f** were repeated independently three times with similar results. Scale bars, 5 μm (**a**–**d**), 2 μm (**e**,**f**) and 1 μm (**g**).

homozygous mutants were indistinguishable from the wild-type control when 1 mM caffeine was included in the growth medium, root growth in the double mutant was greatly retarded when compared to the control and single mutants (Fig. 3b,c). Furthermore, the *bub3;1 bub3;2* mutant had swollen roots and produced giant cells with stained nuclei, indicating failures in cytokinesis (asterisks and arrows, respectively, Fig. 3d). Thus, we conclude that BUB3;1 and BUB3;2 are functionally redundant and only the double homozygous mutant becomes hypersensitive to caffeine. When the double mutant was challenged by caffeine, cytokinesis failures led to retarded root growth.

Because of the BUB3;1–MAP65-3 interaction and the cytokinesis phenotype brought about by the double mutations, we asked whether the BUB3 proteins play a regulatory role in MAP65-3 localization in the phragmoplast. In the *bub3;1 bub3;2* double mutant, MAP65-3 was still detected in the developing phragmoplasts, like in the control cells (Fig. 4a–d). However, MAP65-3 localization in the control cells was mostly restricted to the phragmoplast midline after the establishment of the bipolar microtubule array, whereas its localization in the double mutant became less restricted, with punctate signals along the phragmoplast microtubules (Fig. 4a–d). In the control cells, the MAP65-3 fluorescence occupied the midline where the microtubule signal dropped sharply (Fig. 4e). However, in the double mutant, the MAP65-3 signal had a much wider distribution than the midline before dropping to the basal level (Fig. 4f). Thus, the data indicate that BUB3;1 and BUB3;2 function redundantly in restricting MAP65-3 localization to the phragmoplast midline.

We then asked how the BUB3 protein affected the activity of MAP65-3 in vivo. As reported previously[11], the ectopic expression of cyan fluorescent protein (CFP)-MAP65-3 induced microtubule bundling in epidermal cells of tobacco leaves that otherwise formed a fine microtubule network at the cell cortex (Supplementary Fig. 2). When red fluorescent protein (RFP)-BUB3;1 and CFP-MAP65-3 were co-expressed, microtubules were again heavily bundled and both fusion proteins exhibited localization patterns that were indistinguishable from that of the microtubule bundles highlighted by the GFP-β-tubulin-6 (TUB6) fusion protein (Supplementary Fig. 2). Fluorescence recovery after photobleaching (FRAP) was applied to measure the turnovers of CFP-MAP65-3 on microtubule bundles and revealed that the co-expression of RFP-BUB3;1 greatly decreased the turnover rate of CFP-MAP65-3 (Fig. 4g). Quantitatively, the half-life ($t_{1/2}$) of the fluorescence recovery of the CFP signal after bleaching was averaged at 72.34 s without RFP-BUB3;1 and it was increased to 208.14 s when RFP-BUB3;1 was co-expressed (Fig. 4h). Thus, we concluded that the association of BUB3;1 greatly reduced the turnover rate of MAP65-3 on microtubules.

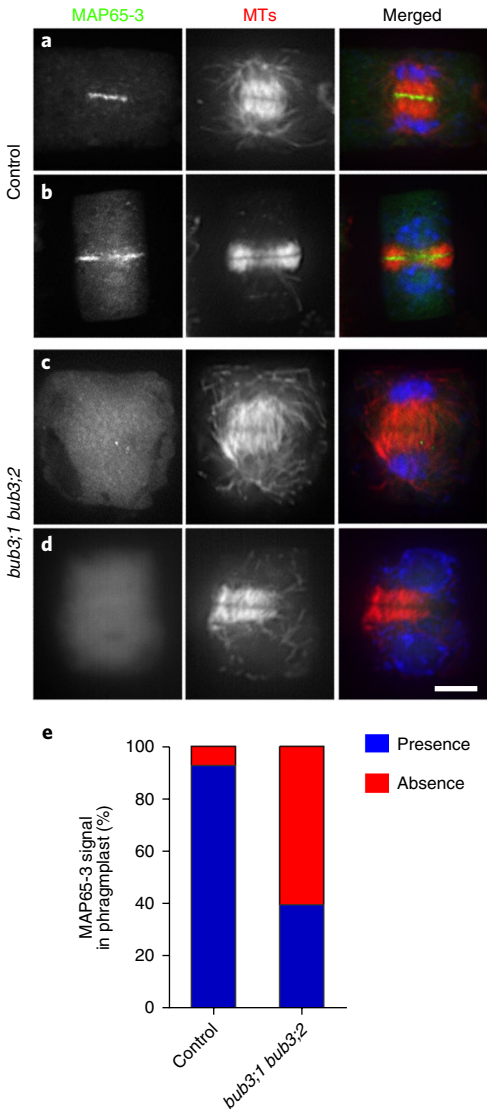

Fig. 5 | Caffeine abolishes MAP65-3 localization in the *bub3* mutant. **a**,**b**, Caffeine treatment does not significantly affect MAP65-3 localization in the control cells. **c**,**d**, After the *bub3;1 bub3;2* cells are treated with 1 mM caffeine, the MAP65-3 signal becomes diffuse in the cytosol and is no longer concentrated in the phragmoplast midline. **e**, Quantitative assessment of the loss of MAP65-3 localization in the phragmoplast in the control ($n = 55$) and mutant ($n = 50$) cells after caffeine treatment. Scale bars, 5 μm (**a**–**d**).

Because of caffeine hypersensitivity in the double mutant, we tested whether the inhibitor affected MAP65-3 localization. When the control roots were treated with 1 mM caffeine for 16 h, MAP65-3 was detected at the midline of developing phragmoplasts of over 90% of the meristematic cells undergoing cytokinesis (Fig. 5a,b). However, in the *bub3;1 bub3;2* double mutant, the MAP65-3 signal was often unnoticeable at the phragmoplast midline at both early and later stages of the phragmoplast (Fig. 5c,d). Quantitatively speaking, approximately 60% of the observed cells undergoing cytokinesis no longer had MAP65-3 conspicuously detected at the phragmoplast midline upon the caffeine challenge, whereas only fewer than 10% of the control cells had the protein localization compromised (Fig. 5e). These results indicate that the cytokinetic defects in the double mutant were a result of compromised MAP65-3 localization when cells were exposed to low doses of caffeine.

Because the *bub3;1 bub3;2* double mutant exhibited cytokinesis defects upon caffeine challenges, we reasoned what could have caused the failure. We first examined microtubule reorganization during cytokinesis in live cells of the control and the double mutant using a GFP-TUB6 fusion protein to mark microtubules (Fig. 6a,b). Upon the assembly of the bipolar phragmoplast microtubule array in the cell centre, the solid array quickly expanded towards the cellular periphery (Supplementary Video 2). In the control cells, the leading edge of the expanding phragmoplast would reach the periphery approximately 12 min after the expansion onset (Fig. 6a). It was noted that the expansion was mostly symmetrical as the edges touched the periphery simultaneously and, in the meantime, microtubules started to depolymerize centrifugally (Fig. 6a and Supplementary Video 2). Approximately 30 min after the expansion started, phragmoplast microtubules were largely disassembled completely.

In the *bub3;1 bub3;2* double mutant cells, the phragmoplast expansion became biased towards one side of the cell (Fig. 6b and Supplementary Video 2). When a middle optical section was taken across the dividing cell, one expanding edge touched the periphery, whereas the other side was still short from reaching the periphery even 18 min after the expansion initiated (Fig. 6b). Eventually, the other expanding edge also reached the periphery, marking the completion of phragmoplast development. Thus, BUB3;1 and BUB3;2 obviously take part in the reorganization of phragmoplast microtubules, probably in the engagement of the antiparallel bundles during the expansion of the array through the positive regulation of the MAP65-3 function in microtubule binding and bundling.

We also examined phragmoplast expansion when the cells were challenged by 1 mM caffeine through the window of microtubules. In the control cells, phragmoplast expansion still took place at a slower pace than those cells that were not exposed to the drug (Supplementary Video 3). However, in the double mutant, phragmoplast expansion was largely halted after the assembly of the microtubule array in the cell centre (Supplementary Video 4). Bundles of microtubules remained at the cell centre for an extended time in dividing cells.

To demonstrate how microtubule organization was affected in the mutant cells when compared to the control, we carried out tubulin immunofluorescence to image phragmoplasts at different stages and compare the mutant and control plants quantitatively. In the control cells, microtubule organization was not obviously altered upon caffeine treatment when compared to the untreated cells (Fig. 6c,d). In the *bub3;1 bub3;2* cells, expanded phragmoplast microtubule arrays were detected towards the later stages of cytokinesis when they were not challenged by caffeine (Fig. 6d). However, towards the later stages of cytokinesis, the phragmoplast microtubule arrays often exhibited asymmetric patterns with obviously more abundant microtubules towards one side than the other (Fig. 6d). Such asymmetry was only occasionally detected in the control plant (Fig. 6g). After the mutant cells were treated with caffeine, microtubule bundles were observed at one side of the cell only or in the middle as if they had came from fragmented phragmoplasts when the daughter nuclei were noticeably formed (Fig. 6f). We categorized mature phragmoplasts into four categories: (1) symmetrically expanded rings, (2) asymmetrically expanded rings, (3) expanded single-sided phragmoplasts and (4) unexpanded defective phragmoplasts (Fig. 6c–f). Without caffeine, the *bub3;1 bub3;2* mutant had approximately 30% of mature phragmoplasts in categories 2 and 3, but were never detected in category 4 (Fig. 6g). However, upon caffeine treatment, only approximately 20% of the mutant phragmoplasts were in category 1, whereas the control had over 80% (Fig. 6g). Thus, we interpret that the failed microtubule reorganization in the phragmoplast upon caffeine treatment is the most likely cause of cytokinesis failure in the mutant cells. These results reveal the function of BUB3 family proteins in microtubule reorganization in the phragmoplast.

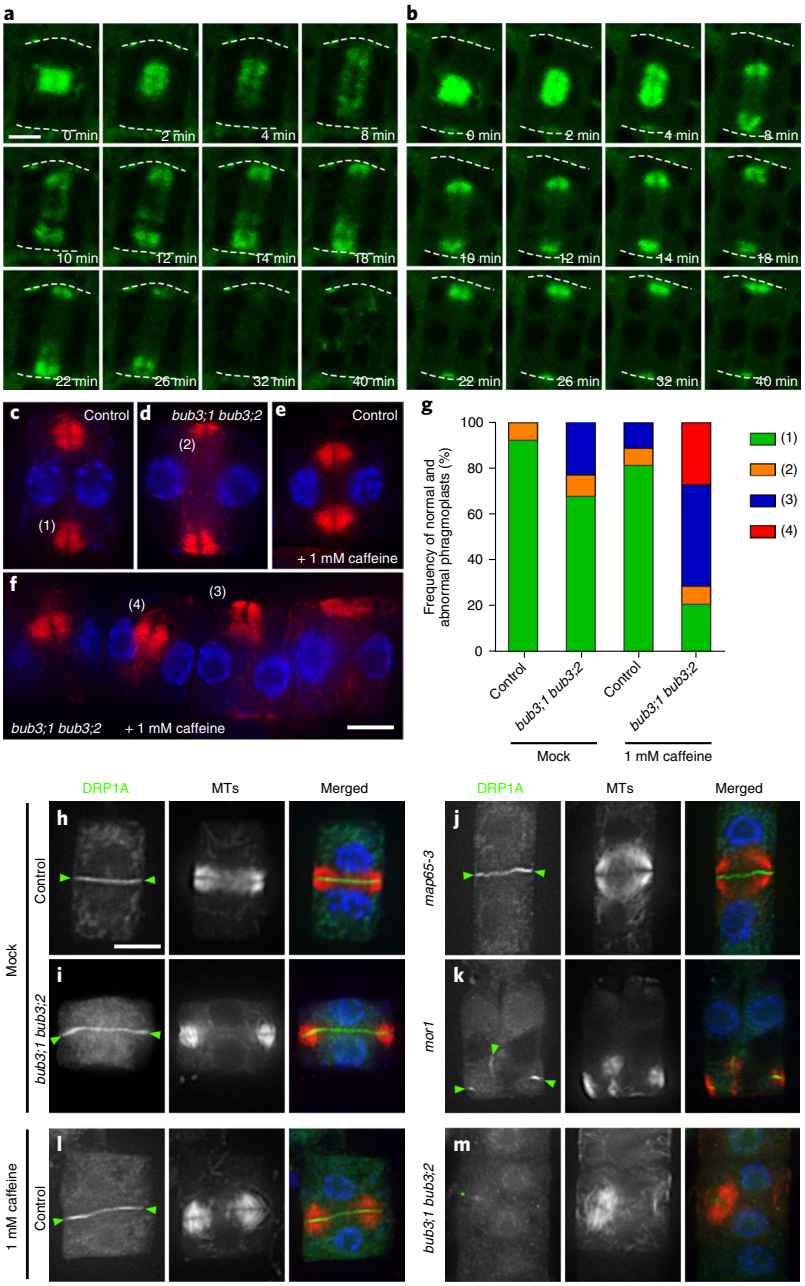

Fig. 6 | BUB3 plays a role in phragmoplast microtubule reorganization. **a**, Reorganization of phragmoplast microtubules marked by GFP-tubulin in a control cell undergoing cytokinesis as illustrated by snapshots at different time points following the onset of phragmoplast expansion. Note that the phragmoplast edge touches the cell periphery ~12 min after the expansion onset. **b**, In the *bub3;1bub3;2* double mutant cell, the phragmoplast microtubule array expands unevenly, with one side reaching the parental membrane at ~8 min after the expansion onset and the other side arriving at ~22 min. Dashed lines indicate lateral edges of cells. **c**–**f**, Mature or late phragmoplast microtubule arrays in control cells (**c**,**e**) and in the *bub3;1bub3;2* double mutant (**d**,**f**), with (**e**,**f**) and without (**c**,**d**) caffeine treatment. The images have the microtubules pseudo-coloured in red and DNA in blue. In control cells, symmetrically expanded phragmoplast microtubule arrays (1) are found in the absence of caffeine (**c**) or after treatment with 1 mM caffeine (**e**). In the double mutant, phragmoplast expansion still takes place without caffeine treatment, but often becomes asymmetric (2) (**d**). After 16-h growth on medium containing 1 mM caffeine, cytokinetic cells have microtubules that are shown like single fragments of phragmoplast either towards the cortex (3) or in the cell centre (4) (**f**). Two of the four cells shown here have the fragment placed near the cell centre (two cells towards the left), whereas the other two cells have the fragment positioned near the cell periphery (two cells on the right) (**f**). **g**, Quantitative assessment of phragmoplast appearance with or without caffeine treatment. The frequencies of four categories of phragmoplasts, as exampled in **c**–**f**, are illustrated for the control sample without caffeine treatment ($n = 65$), the control with caffeine ($n = 53$), the double mutant without caffeine ($n = 54$) and the double mutant with caffeine ($n = 52$). Caffeine treatment greatly increases the frequency of abnormal phragmoplast microtubule arrays in the double mutant. Such an amount of caffeine has little effect on the control cells. **h**–**m**, Cell plate development and triple localization of DRP1A (marking the cell plate), microtubules (MTs) and DNA (shown in blue in the merged images) in control and mutant cells undergoing cytokinesis. Obvious cell plates were detected in the control, *bub3;1bub3;2* double mutant and *map65-3* mutant (arrowheads, **h**–**j**). Pieces of the cell plate were detected within fragmented phragmoplast in the *mor1-1*-mutant cell (arrowheads, **k**). Upon treatment with 1 mM caffeine, the intact cell plate forms in the control cell (arrowheads, **l**), but the DRP1A signal is barely detectable in the *bub3;1bub3;2* double mutant (asterisk, **m**). Experiments in **a**,**b** and **h**–**m** were repeated independently three times with similar results. Scale bars, 5 μm (**a**–**f** and **h**–**m**).

We then asked how cell plate assembly might be affected in the *bub3;1 bub3;2* mutant. Dynamin-related protein 1A (DRP1A)[15] was used as a marker of the developing cell plate to compare the *bub3;1 bub3;2* mutant with other reference plants. We selected cells with two reformed daughter nuclei and a ring-shaped phragmoplast when the cell plate had reached the parental membrane. This is defined as the maturation stage of the cell plate[16]. Mature cell plates were formed in both the *bub3;1 bub3;2* double mutant as well as the *map65-3* mutant, similarly to the control cells before caffeine treatment (Fig. 6h–j). We wished to test whether the defects we observed were similar to the scenario when the overall microtubule organization was challenged. To do so, we used the *mor1-1* mutant grown at the restrictive temperature of 28 °C, at which cells would have the phragmoplast fragmented due to defects in microtubule organization[17,18], and found that pieces of the cell plate were formed in the midzone of the fragmented phragmoplast (Fig. 6k). Upon caffeine treatment, DRP1A was still detected in the control cell, marking the mature cell plate, but became barely detectable within the deformed phragmoplast in the *bub3;1 bub3;2* mutant (Fig. 6l,m). Thus, we concluded that the defects associated with the loss of the BUB3 proteins specifically affect cell plate formation in *A. thaliana*.

Discussion

Our results showed that the highly conserved BUB3 family proteins have evolved to function in phragmoplast-based cytokinesis in *A. thaliana* and most likely other angiosperms as well. Such a function is established through specific interaction between the BUB3;1/BUB3;2 and the MAP65/Ase1p/PRC1 family protein MAP65-3. The BUB3 proteins regulate the association of MAP65-3 with interdigitating microtubules in the phragmoplast midline and, consequently, the initiation and/or expansion of the phragmoplast during cytokinesis. Upon subtle caffeine challenges, the loss of BUB3 led to complete failure of cell plate assembly, a phenotype that has only been synthetically generated in two occasions by combined mutations of *knolle* (encoding syntaxin) and *keule* (encoding Sec1/Munc18), and by *ple-2* (encoding MAP65-3) and *trs120* (encoding transport protein particle II (TRAPPII) subunit)[19,20]. Thus, with the assistance of BUB3, MAP65-3 contributes critically to the initiation of cell plate assembly and later to phragmoplast expansion, which requires the assembly of new 'miniphragmoplast' modules with antiparallel microtubules crosslinked by MAP65-3 at the leading edge[21].

The BUB3 protein is commonly known as an essential docking molecule when the SAC is activated. It forms complexes with both BUB1 and BUBR1 through the interactions with its WD40 repeats, which ensures their localization to unattached kinetochores[2,22]. Consequently, the inactive open MAD2 protein is converted to the active closed MAD2, which joins with BUBR1, BUB3 and cell division cycle protein 20 (CDC20) to form the mitotic checkpoint complex (MCC). Because the MCC sequesters the essential anaphase-promoting complex/cyclosome protein CDC20, mitosis is blocked at prometaphase. In other words, the canonical function of BUB3 is restricted to prometaphase in studied fungal and animal systems. Here, we demonstrated that BUB3;1 and its paralogue BUB3;2 functioned in the developing phragmoplast when mitosis was largely completed. We consider the acquisition of a cytokinesis function for BUB3 as an important event during the evolution towards plants, perhaps concomitantly with the reconstruction or reorganization of the SAC in mitosis; however, to date, solid evidence supporting the presence of the SAC is yet to be provided in angiosperms[5]. Aside from the subcellular localization of BUB3;1/BUB3;2 in the phragmoplast, there are other lines of evidence supporting the notion that the plant BUB3 and the yet-to-be-characterized SAC operate differently from those in fungi and animals. First of all, the inventory of essential SAC regulators is rather complete, together with the MPS1 and Aurora 3 kinases that probably have BUB and MAD proteins as their substrates[23–25]. However, both BUB1 and BUBR1/MAD3 homologues in *A. thaliana* no longer contain the GLEBS domain. Thus, they have lost the foundation to interact with BUB3[24]. Second, the *bub3;1 bub3;2* double mutant reported here did not exhibit a noticeable growth phenotype, indicating that mitosis took place normally during growth and reproduction. This is different from fungi and animals. For example, mutations in the BUB3 orthologue or other SAC regulatory genes lead to severe growth retardation and asexual reproduction defects in the filamentous fungus *Aspergillus nidulans*[26]. BUB3 becomes essential in mammals[4]. Similarly, mutations in another SAC gene, *MAD1*, only cause an early flowering phenotype without noticeably affecting the mitotic progression[27]. Last, BUB1, MAD2 and BUBR1/MAD3 all interact with two of the five CDC20 isoforms in *A. thaliana*[28], perhaps independently to BUB3;1 and BUB3;2 because of their localization after mitosis is completed. It would be interesting to learn what the MCC is made of in angiosperms.

In animals and fungi, BUB3 has been found to interact with the phosphorylated MELT (p-MELT) motifs in the kinetochore scaffolding protein KNL in a cell cycle-dependent manner in addition to interacting with the GLEBS domain in BUBR1/MAD3 and other proteins[22]. Based on the primary amino acid sequences, no obvious KNL1 homologues can be found in *A. thaliana* and other angiosperms. Thus, the GLEBS–BUB3–p-MELT interaction module perhaps does not exist in plants.

In fact, an earlier report suggests that BUB3 is dispensable for mitotic arrest when spindle assembly is perturbed, indicating that it is not required for other core SAC proteins, such as BUBR1/MAD3, to exercise their function on SAC activation in fission yeast[29]. However, unlike what we observed here, the fission yeast BUB3 plays a role in sister centromere cohesion, again, a function that seems to be divergent from assembling the MCC. Unfortunately, the molecular basis of such a non-canonical function of BUB3 is yet to be elucidated. Nevertheless, it represents another example that the functions of BUB3 and SAC-important BUB and MAD proteins may be separate.

The presence of core SAC regulatory proteins makes it hard to deny the presence of an effective SAC system in angiosperms. In fact, the SAC proteins have been detected at the kinetochores in tobacco, maize and wheat cells, especially upon treatments of microtubule-depolymerizing drugs and the 26S proteasome inhibitor MG132[30,31]. However, their functions in the SAC would have to be tested in mutants in which the corresponding genes are inactivated. A recent report showed that the *bmf3* (in a BUBR1-related gene), *mad1* and *mad2* mutants, but not *bub1*/*bmf1* mutants, exhibit hypersensitivity to microtubule-disturbing drugs, which is a signature SAC phenotype[5]. Interestingly, the loss of BUB3;3, the protein that is more divergently related to BUB3 proteins in other kingdoms than BUB3;1 or BUB3;2, also led to oryzalin hypersensitivity[5]. A functional SAC system, following final approval, may operate with input from BUB3;3 instead of BUB3;1 or BUB3;2. It would be informative to elucidate how BUB3;3 may interact with BMF proteins.

Unlike MAP65-3, which is undetectable before mitosis[10], BUB3;1 and BUB3;2 proteins are exclusively localized to the nucleus. Our results demonstrated that it was diffuse in the cytosol following nuclear envelope breakdown and only became associated with the microtubules after being recruited by MAP65-3 to decorate antiparallel microtubules. Perhaps their function is restricted to regulating MAP65-3 activity. The phragmoplast-based cytokinesis mechanism differs from those mechanisms involving the actomyosin contractile ring, which is uniquely featured by the assembly of the cell plate and the deposition of the new cross wall that separates two daughter cells following vesicle transport, fusion and fission. The participation of BUB3 may represent a specialized feature in this process, even though both the BUB3 and the MAP65 family proteins are well conserved across kingdoms.

In the *bub3;1 bub3;2* mutant, the expansion of the phragmoplast microtubule array was affected when the MAP65-3 protein became less concentrated at the midline. Our results indicate that the two BUB3 proteins function in modulating the concentration of the microtubule-associated protein to the microtubule-overlapping segment towards the microtubule plus ends by enhancing MAP65-3 association with microtubules. To date, it has only been reported that the activity of the MAP65 and PRC1 family proteins for bundling antiparallel microtubules during telophase and cytokinesis may be regulated by protein phosphorylation[32,33]. In flowering plants, a mitogen-activated protein kinase (MAPK) cascade plays a critical role in cytokinesis by phosphorylating MAP65[34]. Phosphorylation of MAP65 by this MAPK cascade compromises its microtubule-bundling activity, which promotes microtubule turnovers during phragmoplast expansion in tobacco cells[35]. In *A. thaliana*, MAP65-3 is also phosphorylated by MAPK[36]. Thus, our findings uncovered the first mechanism of positive regulation of MAP65-3 activities in the phragmoplast.

The BUB3;1 and BUB3;2 proteins positively regulate MAP65-3 binding to microtubules so that they could facilitate the MAP65-3-mediated engagement of antiparallel microtubules during phragmoplast expansion. In this process, newly polymerized microtubules from two halves of the phragmoplast are captured by MAP65 proteins at the expanding periphery[37]. If we view the phragmoplast as an assembly of miniphragmoplast modules made of interdigitating core microtubules plus surrounding non-interdigitating microtubules[21], the establishment of newly interdigitated microtubules marks the establishment of new miniphragmoplast modules. Although MAP65-3 itself is sufficient to dimerize to bundle antiparallel microtubules in vitro[10], the input from BUB3 would perhaps facilitate the establishment of the miniphragmoplast because of its recruitment by MAP65-3 through the interaction with its microtubule-binding site. In the absence of BUB3;1 and BUB3;2, MAP65-3 would still crosslink antiparallel microtubules but became vulnerable to challenges, such as low doses of caffeine, so that the phragmoplast would fail to expand. Stabilization of microtubule interdigitation may also depend on the concentration of MAP65 proteins. For example, we recently showed that MAP65-4, which is functionally redundant with MAP65-3, although far less important, was able to suppress the loss-of-function mutation of MAP65-3 upon elevated expressions[38]. This hypothesis is supported by the phenotype of more dispersed localization of MAP65-3 along phragmoplast microtubules in the absence of BUB3;1/BUB3;2. Collectively, stabilization of the newly crosslinked antiparallel microtubules positively contributes to the rapid expansion of the phragmoplast microtubule array during cytokinesis.

During phragmoplast expansion, microtubule reorganization is coupled with membrane remodelling for cell plate assembly. Besides being microtubule-bundling factors, MAP65 isoforms have been demonstrated to interact with the TRAPPII tethering factors, providing a direct link between microtubule dynamics and membrane trafficking in the phragmoplast[19]. Because MAP65 proteins are substrates of at least three classes of kinases—Aurora, cyclin-dependent kinase and MAPK—its interaction with TRAPPII is hypothesized to be a link of cell cycle progress to cell plate assembly[39]. Here, we demonstrated that the nuclear protein BUB3 became associated with MAP65-3 later in cell division to regulate its microtubule-bundling activity. Thus, the action of BUB3 perhaps also delivers cell cycle-dependent, nucleus-initiated information that signals the initiation of cell plate assembly.

The phragmoplast represents a cytokinesis mechanism that is found among advanced green algae and plants, in contrast to the actomyosin contractile ring-based mechanism that is found among many protists as well as fungi and animals. The inhibition of the expansion process in the mutant suggests that perhaps the WD40 repeat protein has been used by the phragmoplast as part of the machinery that warrants the remodelling of the phragmoplast apparatus during cytokinesis. Considering the essential inputs of the nucleus, phragmoplast microtubules and the membranous compartment for the final assembly of the cell plate, perhaps BUB3 might be a critical player that ties them together. Hence, our discovery of the novel function of BUB3 in phragmoplast-based cytokinesis invites further investigations of the significance of such a seemingly non-canonical role among other organisms that use the phragmoplast for cytokinesis.

Methods

Plant materials and growth conditions. All *A. thaliana* plants described here are in the Columbia background. The *bub3;1*- and *bub3;2*-mutant plants were isolated from the seed stocks of the SK29246 (CS1009817) and SALK_151687C lines, respectively, that were made available to us by the Arabidopsis Biological Research Center (ABRC) at Ohio State University in Columbus, Ohio, USA. The primers used for genotyping are listed in Supplementary Table 1. The LP and RP primer pairs were used for detecting the wild-type allele of the corresponding genes. The *bub3;1* T-DNA insertional mutation was detected by the primer pair of 1009817RP and SKTAIL-L1, and SALK_151687C by 151687RP and LBa1, with the wild-type plant as the negative control. The *mor1-1* mutant was ordered from the ABRC and the *map65-3* was as previously reported[40]. All plants were grown in the growth chamber at 21 °C with 16-h light and 8-h dark cycles as previously described[41]. Live-cell imaging was carried out using young seedlings produced on solid medium supplied with 1/2 Murashige Skoog salt mixture.

Constructs for the expression of two BUB3-GFP fusion proteins as well as markers were delivered into *A. thaliana* with corresponding genotypes via *Agrobacterium*-mediated transformation using the standard floral dipping method. Transgenic plants were selected on antibiotic markers carried by respective vectors. The tobacco *Nicotiana benthamiana* was used for transient expression experiments through agrobacterial infiltration as described in our previous work[11].

Recombinant DNA manipulations and plasmid construction. To produce the BUB3;1-GFP and the BUB3;2-GFP expression constructs, DNA fragments containing both the promoter and the coding regions were amplified from wild-type genomic DNA by the Phusion DNA polymerase (Thermo Fisher) using primer pairs of BUB31F–BUB31R and BUB32Fn–BUB32Rn, respectively. The amplified fragments were cloned into a gateway entry vector using the pENTR/D-Topo cloning kit (Thermo Fisher). The resulting pENTR clones were recombined with pGWB4 or pGWB650[42,43] by the LR recombinase following the manufacturer's instructions to give rise to the final expression constructs.

The constructs for the BiFC test were produced as follows. The BUB3;1 complementary DNA fragment was amplified using the U50094 plasmid (ABRC) as the template by the primers of BUB3BiFC5 and BUB31R. Following restriction enzyme digestion, the cDNA was inserted into the expression vector pSPDK919 at the MluI and XbaI sites to express BUB3;1-cCitrine. The MAP65-3-nCitrine and MAP65-1-nCitrine constructs were described previously[11].

Fluorescent microscopy. The localization of BUB3 family proteins was determined in root meristematic cells. For live-cell observation, 3–5-day-old seedlings grown on agar medium supplied with 1/2 Murashige Skoog salt were transferred to glass slides and submerged in water. Root cells were observed under an Axio Observer inverted microscope equipped with the LSM710 laser scanning confocal module with standard settings for eGFP and mCherry (Carl Zeiss). A ×40 C-Plan (water) or ×63 Plan-Apo (oil) objective was used, and images were acquired using the ZEN software package (Carl Zeiss) and processed in ImageJ (www.imagej.nih.gov/ij).

In the BiFC tests, constructs were transiently expressed in leaf cells of *N. benthamiana* following agrobacterial infiltration. Sliced leaf segments were observed using the LSM710 confocal microscope as described above. FRAP was carried out according to settings included in LSM710 using a 405-nm laser.

For immunolocalization, meristematic cells derived from root tips were used according to previously described protocols[44]. The primary antibodies used in this study were monoclonal mouse anti-GFP antibodies (Covance), polyclonal sheep anti-tubulin antibodies (Cytoskeleton), polyclonal anti-DRP1A antibodies[15] and polyclonal rabbit anti-MAP65-3[10]. Secondary antibodies were fluorescein isothiocyanate (FITC)-conjugated donkey anti-mouse IgG, FITC-conjugated donkey anti-rabbit IgG and Texas Red-conjugated donkey anti-goat IgG (Rockland Immunochemicals). Fluorescently labelled cells were observed under an Eclipse 600 microscope equipped with ×60 Plan-Apo and ×100 Plan-Fluor objectives (Nikon), and images were acquired by an OptiMOS camera (Q Imaging) controlled by the μManager software package[45,46].

Reporting Summary. Further information on experimental design is available in the Nature Research Reporting Summary linked to this article.

Data availability. The data sets generated during and/or analysed during the current study are available from the corresponding author on reasonable request.

The Arabidopsis Information Resource locus identifier recognizes the genes mentioned in this article as At3g19590 for *BUB3;1* and At1g49910 for *BUB3;2*.

Received: 14 September 2017; Accepted: 4 June 2018;
Published online: 2 July 2018

References

1. Hoyt, M. A., Totis, L. & Roberts, B. T. *S. cerevisiae* genes required for cell cycle arrest in response to loss of microtubule function. *Cell* **66**, 507–517 (1991).
2. Musacchio, A. The molecular biology of spindle assembly checkpoint signaling dynamics. *Curr. Biol.* **25**, R1002–R1018 (2015).
3. Li, R. & Murray, A. W. Feedback control of mitosis in budding yeast. *Cell* **66**, 519–531 (1991).
4. Babu, J. R. et al. Rae1 is an essential mitotic checkpoint regulator that cooperates with Bub3 to prevent chromosome missegregation. *J. Cell Biol.* **160**, 341–353 (2003).
5. Komaki, S. & Schnittger, A. The spindle assembly checkpoint in *Arabidopsis* is rapidly shut off during severe stress. *Dev. Cell* **43**, 172–185.e5 (2017).
6. Lermontova, I., Fuchs, J. & Schubert, I. The *Arabidopsis* checkpoint protein Bub3.1 is essential for gametophyte development. *Front Biosci.* **13**, 5202–5211 (2008).
7. Van Leene, J. et al. Targeted interactomics reveals a complex core cell cycle machinery in *Arabidopsis thaliana*. *Mol. Syst. Biol.* **6**, 397 (2010).
8. Smertenko, A. P. et al. The C-terminal variable region specifies the dynamic properties of *Arabidopsis* microtubule-associated protein MAP65 isotypes. *Plant Cell* **20**, 3346–3358 (2008).
9. Müller, S. et al. The plant microtubule-associated protein AtMAP65-3/PLE is essential for cytokinetic phragmoplast function. *Curr. Biol.* **14**, 412–417 (2004).
10. Ho, C. M. et al. Interaction of antiparallel microtubules in the phragmoplast is mediated by the microtubule-associated protein MAP65-3 in *Arabidopsis*. *Plant Cell* **23**, 2909–2923 (2011).
11. Ho, C. M., Lee, Y. R., Kiyama, L. D., Dinesh-Kumar, S. P. & Liu, B. *Arabidopsis* microtubule-associated protein MAP65-3 cross-links antiparallel microtubules toward their plus ends in the phragmoplast via its distinct C-terminal microtubule binding domain. *Plant Cell* **24**, 2071–2085 (2012).
12. Smertenko, A. P. et al. The *Arabidopsis* microtubule-associated protein AtMAP65-1: molecular analysis of its microtubule bundling activity. *Plant Cell* **16**, 2035–2047 (2004).
13. Lee, Y. J. et al. The mitotic function of augmin is dependent on its microtubule-associated protein subunit EDE1 in *Arabidopsis thaliana*. *Curr. Biol.* **27**, 3891–3897.e4 (2017).
14. Hepler, P. K. & Bonsignore, C. L. Caffeine inhibition of cytokinesis—ultrastructure of cell plate formation degradation. *Protoplasma* **157**, 182–192 (1990).
15. Kang, B. H., Busse, J. S. & Bednarek, S. Y. Members of the *Arabidopsis* dynamin-like gene family, ADL1, are essential for plant cytokinesis and polarized cell growth. *Plant Cell* **15**, 899–913 (2003).
16. Smertenko, A. et al. Plant cytokinesis: terminology for structures and processes. *Trends Cell Biol.* **27**, 885–894 (2017).
17. Eleftheriou, E. P., Baskin, T. I. & Hepler, P. K. Aberrant cell plate formation in the *Arabidopsis thaliana microtubule organization 1* mutant. *Plant Cell Physiol.* **46**, 671–675 (2005).
18. Steiner, A. et al. The membrane-associated Sec1/Munc18 KEULE is required for phragmoplast microtubule reorganization during cytokinesis in *Arabidopsis*. *Mol. Plant* **9**, 528–540 (2016).
19. Steiner, A. et al. Cell cycle-regulated PLEIADE/AtMAP65-3 links membrane and microtubule dynamics during plant cytokinesis. *Plant J.* **88**, 531–541 (2016).
20. Waizenegger, I. et al. The *Arabidopsis KNOLLE* and *KEULE* genes interact to promote vesicle fusion during cytokinesis. *Curr. Biol.* **10**, 1371–1374 (2000).
21. Lee, Y. R. & Liu, B. The rise and fall of the phragmoplast microtubule array. *Curr. Opin. Plant Biol.* **16**, 757–763 (2013).
22. London, N. & Biggins, S. Signalling dynamics in the spindle checkpoint response. *Nat. Rev. Mol. Cell Biol.* **15**, 736–747 (2014).
23. Ding, D., Muthuswamy, S. & Meier, I. Functional interaction between the *Arabidopsis* orthologs of spindle assembly checkpoint proteins MAD1 and MAD2 and the nucleoporin NUA. *Plant Mol. Biol.* **79**, 203–216 (2012).
24. Komaki, S. & Schnittger, A. The spindle checkpoint in plants—a green variation over a conserved theme? *Curr. Opin. Plant Biol.* **34**, 84–91 (2016).
25. Van Damme, D. et al. *Arabidopsis* α Aurora kinases function in formative cell division plane orientation. *Plant Cell* **23**, 4013–4024 (2011).
26. Efimov, V. P. & Morris, N. R. A screen for dynein synthetic lethals in *Aspergillus nidulans* identifies spindle assembly checkpoint genes and other genes involved in mitosis. *Genetics* **149**, 101–116 (1998).
27. Bao, Z., Zhang, N. & Hua, J. Endopolyploidization and flowering time are antagonistically regulated by checkpoint component MAD1 and immunity modulator MOS1. *Nat. Commun.* **5**, 5628 (2014).
28. Kevei, Z. et al. Conserved CDC20 cell cycle functions are carried out by two of the five isoforms in *Arabidopsis thaliana*. *PLoS ONE* **6**, e20618 (2011).
29. Tange, Y. & Niwa, O. *Schizosaccharomyces pombe* Bub3 is dispensable for mitotic arrest following perturbed spindle formation. *Genetics* **179**, 785–792 (2008).
30. Caillaud, M. C. et al. Spindle assembly checkpoint protein dynamics reveal conserved and unsuspected roles in plant cell division. *PLoS ONE* **4**, e6757 (2009).
31. Yu, H. G., Muszynski, M. G. & Kelly Dawe, R. The maize homologue of the cell cycle checkpoint protein MAD2 reveals kinetochore substructure and contrasting mitotic and meiotic localization patterns. *J. Cell Biol.* **145**, 425–435 (1999).
32. Hu, C. K., Ozlu, N., Coughlin, M., Steen, J. J. & Mitchison, T. J. Plk1 negatively regulates PRC1 to prevent premature midzone formation before cytokinesis. *Mol. Biol. Cell* **23**, 2702–2711 (2012).
33. Smertenko, A. P. et al. Control of the AtMAP65-1 interaction with microtubules through the cell cycle. *J. Cell Sci.* **119**, 3227–3237 (2006).
34. Sasabe, M. & Machida, Y. Regulation of organization and function of microtubules by the mitogen-activated protein kinase cascade during plant cytokinesis. *Cytoskeleton (Hoboken)* **69**, 913–918 (2012).
35. Nishihama, R. et al. Expansion of the cell plate in plant cytokinesis requires a kinesin-like protein/MAPKKK complex. *Cell* **109**, 87–99 (2002).
36. Kosetsu, K. et al. The MAP kinase MPK4 is required for cytokinesis in *Arabidopsis thaliana*. *Plant Cell* **22**, 3778–3790 (2010).
37. Murata, T. et al. Mechanism of microtubule array expansion in the cytokinetic phragmoplast. *Nat. Commun.* **4**, 1967 (2013).
38. Li, H. et al. *Arabidopsis* MAP65-4 plays a role in phragmoplast microtubule organization and marks the cortical cell division site. *New Phytol.* **215**, 187–201 (2017).
39. Ravikumar, R., Steiner, A. & Assaad, F. F. Multisubunit tethering complexes in higher plants. *Curr. Opin. Plant Biol.* **40**, 97–105 (2017).
40. Sasabe, M., Kosetsu, K., Hidaka, M., Murase, A. & Machida, Y. *Arabidopsis thaliana* MAP65-1 and MAP65-2 function redundantly with MAP65-3/PLEIADE in cytokinesis downstream of MPK4. *Plant Signal. Behav.* **6**, 743–747 (2011).
41. Kong, Z., Hotta, T., Lee, Y. R., Horio, T. & Liu, B. The γ-tubulin complex protein GCP4 is required for organizing functional microtubule arrays in *Arabidopsis thaliana*. *Plant Cell* **22**, 191–204 (2010).
42. Nakamura, S. et al. Gateway binary vectors with the bialaphos resistance gene, *bar*, as a selection marker for plant transformation. *Biosci. Biotechnol. Biochem.* **74**, 1315–1319 (2010).
43. Nakagawa, T. et al. Development of series of gateway binary vectors, pGWBs, for realizing efficient construction of fusion genes for plant transformation. *J. Biosci. Bioeng.* **104**, 34–41 (2007).
44. Lee, Y. R. J. & Liu, B. Identification of a phragmoplast-associated kinesin-related protein in higher plants. *Curr. Biol.* **10**, 797–800 (2000).
45. Edelstein, A., Amodaj, N., Hoover, K. & Vale, R. Computer control of microscopes using μManager. *Curr. Protoc. Mol. Biol.* **92**, 14.20.1–14.20.17 (2010).
46. Edelstein, A. D. et al. Advanced methods of microscope control using μ Manager software. *J. Biol. Methods* **1**, e10 (2014).

Acknowledgements

We thank members of the Liu laboratory for critical comments on the work. Special thanks go to S. P. Dinesh-Kumar for the BiFC vectors and T. Nakagawa at Shimane University in Japan for the pGWB plasmids, and S. Bednarek for the DRP1A antibody. This work was supported by the US National Science Foundation under the grant MCB-1412509 to B.L. and Y.-R.J.L. H.Z. was supported by a fellowship from the China Scholarship Council (no. 201406305055), the Fundamental Research Funds for the Central Universities (no. 2452018155) and the 111 Project from the Ministry of Education of China (no. B07049). Any opinions, findings and conclusions or recommendations expressed in this material are those of the authors and do not necessarily reflect the views of the funding agency.

Author contributions

Y.-R.J.L. and B.L. conceived the project and designed the experiments. H.Z., X.D., B.S., S.L.V. and Y.-R.J.L. performed the experiments. H.Z., X.D., Z.K., H.L., Y.-R.J.L. and B.L. analysed the data and interpreted the results. Y.-R.J.L. and B.L. wrote the manuscript with inputs from other authors.

Competing interests

The authors declare no competing interests.

Additional information

Supplementary information is available for this paper at https://doi.org/10.1038/s41477-018-0192-z.

Correspondence and requests for materials should be addressed to Y.-R.J.L. or B.L.

nature research

Corresponding author(s): Bo Liu

Reporting Summary

Nature Research wishes to improve the reproducibility of the work that we publish. This form provides structure for consistency and transparency in reporting. For further information on Nature Research policies, see Authors & Referees and the Editorial Policy Checklist.

Statistical parameters

When statistical analyses are reported, confirm that the following items are present in the relevant location (e.g. figure legend, table legend, main text, or Methods section).

n/a	Confirmed	
☐	☒	The exact sample size (*n*) for each experimental group/condition, given as a discrete number and unit of measurement
☐	☒	An indication of whether measurements were taken from distinct samples or whether the same sample was measured repeatedly
☒	☐	The statistical test(s) used AND whether they are one- or two-sided *Only common tests should be described solely by name; describe more complex techniques in the Methods section.*
☒	☐	A description of all covariates tested
☒	☐	A description of any assumptions or corrections, such as tests of normality and adjustment for multiple comparisons
☒	☐	A full description of the statistics including central tendency (e.g. means) or other basic estimates (e.g. regression coefficient) AND variation (e.g. standard deviation) or associated estimates of uncertainty (e.g. confidence intervals)
☒	☐	For null hypothesis testing, the test statistic (e.g. *F*, *t*, *r*) with confidence intervals, effect sizes, degrees of freedom and *P* value noted *Give P values as exact values whenever suitable.*
☒	☐	For Bayesian analysis, information on the choice of priors and Markov chain Monte Carlo settings
☒	☐	For hierarchical and complex designs, identification of the appropriate level for tests and full reporting of outcomes
☒	☐	Estimates of effect sizes (e.g. Cohen's *d*, Pearson's *r*), indicating how they were calculated
☐	☒	Clearly defined error bars *State explicitly what error bars represent (e.g. SD, SE, CI)*

Our web collection on statistics for biologists may be useful.

Software and code

Policy information about availability of computer code

Data collection	Micro-Manager version 1.4 (Open Imaging, Inc.) and ZEN (Carl Zeiss) software packages were used in image collection.
Data analysis	ImageJ (National Institutes of Health, USA) was used in image analysis.

For manuscripts utilizing custom algorithms or software that are central to the research but not yet described in published literature, software must be made available to editors/reviewers upon request. We strongly encourage code deposition in a community repository (e.g. GitHub). See the Nature Research guidelines for submitting code & software for further information.

Data

Policy information about availability of data

All manuscripts must include a data availability statement. This statement should provide the following information, where applicable:

- Accession codes, unique identifiers, or web links for publicly available datasets
- A list of figures that have associated raw data
- A description of any restrictions on data availability

All genetic materials reported in this manuscript will be made available to the community upon request and signing the material transfer agreement with our home institution.

Field-specific reporting

Please select the best fit for your research. If you are not sure, read the appropriate sections before making your selection.

☒ Life sciences ☐ Behavioural & social sciences ☐ Ecological, evolutionary & environmental sciences

For a reference copy of the document with all sections, see nature.com/authors/policies/ReportingSummary-flat.pdf

Life sciences study design

All studies must disclose on these points even when the disclosure is negative.

Sample size	Sample sizes were at least 10 per sample. In all experimental results presented in the manuscript, the differences were obvious as indicated by clear differences in all comparisons of the bub3;1 bub3;2 and the wild type control or complemented lines.
Data exclusions	No data were excluded.
Replication	All attempts at replication were successful.
Randomization	Samples were separated by their genetic backgrounds. Within each genetic makeup, results were collected from random cells.
Blinding	Blinding was repeated at least three times to verify the phenotypes associated with the mutant when investigators observed cells prepared from different genetic backgrounds.

Reporting for specific materials, systems and methods

Materials & experimental systems

n/a	Involved in the study
☐	☒ Unique biological materials
☐	☒ Antibodies
☒	☐ Eukaryotic cell lines
☒	☐ Palaeontology
☒	☐ Animals and other organisms
☒	☐ Human research participants

Methods

n/a	Involved in the study
☒	☐ ChIP-seq
☒	☐ Flow cytometry
☒	☐ MRI-based neuroimaging

Unique biological materials

Policy information about availability of materials

Obtaining unique materials	The bub3;1, bub3;2, and bub3;2 bub3;2 mutant lines of the plant Arabidopsis thaliana.

Antibodies

Antibodies used	monoclonal mouse anti-GFP antibody from Covance, Catalog number MMS-118P. polyclonal sheep anti-tubulin antibodies from Cytoskeleton, Inc., catalog number ATN02. polyclonal rabbit anti-DRP1A antibodies from Kang et al., 2003. Plant Cell 15, 899-913 polyclonal rabbit anti-MAP65-3 antibodies from Ho et al., 2011. Plant Cell 23, 2909-2923. secondary antibody FITC-conjugated donkey anti-rabbit IgG from Rockland Antibodies & Assays, catalog number 611-702-127. secondary antibody Texas Red–conjugated donkey anti-mouse IgG from Rockland Antibodies & Assays, catalog number 610-709-124. secondary antibody FITC- conjugated donkey anti-mouse IgG from Rockland Antibodies & Assays, catalog number 610-702-124. secondary antibody Texas Red–conjugated donkey anti-sheep IgG from Rockland Antibodies & Assays, catalog number 613-709-168.
Validation	The anti-GFP and anti-tubulin antibodies were validated by the respective manufacturers as stated in their website. The anti-DRP1A and MAP65-3 antibodies were validated in the respective original articles that demonstrated specificities by immunoblotting and immunofluorescence experiments.